4D Modeling of the Lung by Registering Orthogonal Unsynchronized MR Images

Takase, F. K.
University of São Paulo
fktakase@usp.br

Tsuzuki, M. S. G.
University of São Paulo
mtsuzuki@usp.br

Gotoh, T.
Yokohama National University

Kagei, S.
Yokohama National University

Asakura, A.
Yokohama National University

Iwasawa, T.
Kanagawa Cardiovascular and Respiratory Center

Abstract. *This work discusses a 4D lung reconstruction method from unsynchronized MR sequential images. When a chest surgery is done, the lung stops its movements, turning impossible to directly observe the motion of the lung. The visualization of lung movement is a current challenge in medicine. The lung's movement is not periodic and is susceptible to variations in the degree of respiration. Compared to CT, MR imaging involves longer acquisition times and it is not possible to obtain instantaneous 3D images of the lung. For each slice, only one temporal sequence of 2D images can be obtained. However, methods using MR are preferable because they do not involve radiation. In this work, based on unsynchronized sequences of MR images an animated B-Rep solid model is created. For each different obtained sequence of MR images a distinct animated B-Rep solid model is created. The considered method is divided in two parts: firstly, the lung's silhouettes moving in time are extracted by detecting the presence of a respiratory pattern on 2D spatio–temporal MR images. This approach enables the determination of the lung's silhouette for every frame, even on frames with obscure edges. The sequences of extracted lung's silhouettes are unsynchronized sagittal and coronal silhouettes. As a result of the animated silhouette extraction algorithm, the animated silhouette is represented as a scaled lung model. Registering orthogonal silhouettes creates a lung wire frame model. The wire-frame creation problem is severely underconstrained, as many surfaces could give rise to the observed silhouettes. One silhouette type is used as guide and the other silhouette type defines the 3D model. The silhouette composition algorithm uses the registration method for orthogonal silhouettes, which is based on the search for the scale that correctly composes the orthogonal silhouettes. Finally, a B-Rep solid model is created using a meshing algorithm. In the shaded model, it is also possible to recognize some 3D characteristics, for the right and left lungs.*

Keywords: *4D MRI, Animated Lung Visualization, Lung's Volume in Time, Lung Image, B-Rep, Bézier*

1. Introduction

MR imaging of the lung is limited by the low signal-to-noise ratio (SNR) due to the low proton density of the air (Ko and Naidich, 2004). The low SNR demands longer acquisition time for each image and shortening the acquisition time yields lower spatial resolution. Thus, recent lung MR imaging sequence developments have focused on the functional aspects of the lung, such as ventilation and perfusion, and on lesion characterization, all of which can be evaluated predominantly at MR imaging with low spatial resolution (Mills et al., 2003). The knowledge of the lung volume is of special interest and approaches to obtain this knowledge were proposed. One approach to evaluate the lung volume is related to the observation of the diaphragm. Clutzel et al. (2000) managed to obtain a 3D MRI of a breath holding lung shortening the exposition time for each image. The image sequence was used to measure the diaphragmatic area as well as the relationship between the diaphragmatic area and the lung volume. Gauthier et al. (1994) evaluated not only the area of the diaphragm but also the shape of the diaphragm at different lung volumes and Gierada et. al. (1995) considered the diaphragmatic motion using sequential MR images taken during quiet breathing. Iwasawa et al. (2002) quantitatively evaluated the diaphragmatic motion using MR imaging from the displacement area and the total diaphragmatic movement

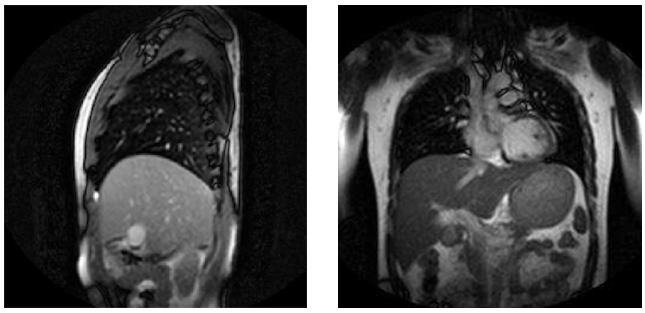

(a) Sagittal image. (b) Coronal image.

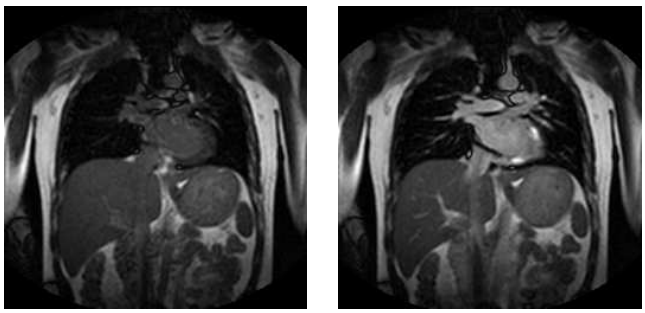

(c) Coronal image. (d) Coronal image.

Figure 1. Samples of MR images. (a) shows a sagittal image. (b) shows the ascending aorta. (c) and (d) show different instants in time of the same slice.

in a respiratory cycle. Another approach tried to relate the lung volume to the chest wall motion retrieved from MRI sequences (Cluzel et al., 2000; Gauthier et al., 1994; Gierada et al., 1995; Suga et al., 1999).

Lung deformations have been studied for the verification of medical imaging equipments and for medical training purposes. The initial methods to model the lung deformation were based on physiology and clinical measurements. The deformation of the lung model as a linear model was proposed by Promayon et al. (1997). A non-physically-based method to describe lung deformations was proposed using NURBS surfaces based on imaging data from CT scans of actual patients (Tsui et al., 2000). Zordan et al. created an anatomical inspired, physically based model of human torso for the visual simulation of respiration (Zordan et al., 2004). To obtain 3D information about the lung from MRI images the boundaries of the lung in each image should be retrieved. Ray et al. (2003) proposed the segmentation of the image by merging parametric contours within homogeneous image regions. In this work a 4D lung model is retrieved from a sequence of MR images taken from a breathing lung. This is accomplished through the analysis of the respiratory motion of the lung boundaries. DeCarlo et al. (1995) examined the Finite Element Method implementation of a two-dimensional idealized lung.

2. Background

Figure 1.(a) shows an example of MR sagittal image. It is possible to process the image shown in Figure 1.(a) using the methods present in the literature (for example, the Sobel operator), the lung's silhouette is very clear and the heart is not present. Figure 1.(b) shows a coronal image with the presence of the ascending aorta, where it is possible to extract the silhouette of the lung automatically using a specific knowledge. Figure 1.(c) shows an example of a blurred image of the chest, where bronchi and large vessels are present. It is very difficult to determine the silhouette of the lung in this case. The knowledge of a medical doctor is necessary in the definition of the lung's silhouette. Figures 1.(c) and 1.(d) show different instants in time of the same slice, the number of vessels inside the lung can vary very much in time, even for the same slice.

The lung motion is caused by the following mechanism. The intercostals muscles around the rib-cage move forward, and the diaphragm, the muscle beneath the lungs, moves downward simultaneously. These movements cause the pressure changes in the pleural cavity surrounding the lungs and the alveoli thus allowing the air from the atmosphere to flow inside the lungs. The packing and unpacking of the alveoli during inspiration and expiration causes surface tension to decrease and increase in a manner that produces the characteristic hysteresis of the lungs. Hysteresis means that inflation of the lung follows a different pressure/volume relationship from deflation (Santhanam et al., 2004). Then, the respiration has two phases: inspiratory and expiratory.

Figure 2. Two disjoint intersecting images from the same lung. The mismatch is more evident on the contour of the diaphragmatic surface.

2.1 Problem Statement

Accurate three-dimensional description of internal organs may be generated using surface based approaches for the segmentation of a stack of images - a volumetric intensity map of this organ. Those voxel based descriptions may be generated from a set of MR images only for non-moving and non-deforming internal structures, as the MR imaging process is slow and the construction of this volumetric description must happen in a slice-to-slice based registration process. In the case of the lung, a sound three dimensional volumetric description can not be builded through the use of both a large set of MR images and a good registration method, because each image Ims, t_i of each slice s is taken in a different time instant t_i, with the lung at different stages of the inflating/deflating process. This situation is illustrated in Figure 2 where two disjointed intersecting images (coronal and sagittal) of the lung are shown.

This dazed situation is aggravated by the pulsating polarization disturbance caused by the heartbeat, which harshes the registration of images taken from the same slice. In Figure 1(c) and (d) two coronal images taken from the same slice of the lung at different time instants are shown.

In this work, it was presented an approach for the lung image segmentation for two-dimensional parametric boundary retrieval, an approach that allows the three-dimensional reconstruction of the lung at different respiratory instants.

2.2 Respiratory Function

Considering a time sequence of MR images from a slice s of the lung, this time-ordered sequence of images may be stacked, defining a spatio-temporal volume (STV) $I_s(x, y, t)$ where x and y are the coordinates of each pixel of the image and t is the time of the image acquisition. Figure 3 shows an example of an STV, builded from 10 coronal images from the same slice of the lung taken in different time instants.

A plane $Q_s(x_s, y_s, \theta_s)$ that pass on point (x_s, y_s), makes an angle of θ_s with the x axis and is parallel to the time axis is defined. Figure 4.(a) shows a chest MR image with three different planes $Q_s(x_s, y_s, \theta_s)$ represented ($\theta_s = 90^o$, $\theta_s = 0^o$ and $\theta_s = 45^o$). Plane $Q_s(x_s, y_s, \theta_s)$ defines a 2D spatio-temporal (2DST) image $F_s(\chi, t)$. Figures 4.(a), 4.(b) and 4.(c) show vertical, horizontal and oblique 2DST images, respectively.

A standard respiratory function is extracted from plane $Q_s(x_s, y_s, 90^o)$ with 2DST image $F_s(y, t)$. Figure 4.(d) shows an example of standard respiratory function that was extracted from the region indicated by an arrow in Figure 4.(a). The standard respiratory function is represented as $\chi = f_s(t)$ over the 2DST image. The value of $F_s(y, t)$ with lowest y is defined as ξ_s and the correspondent instant in time is given by τ_s. This special point (ξ_s, τ_s) defines the origin of the 2DST image. This way, it is possible to map the coordinates of the 2DST image $F_s(\chi, t)$ with the original STV $I_s(x, y, t)$

$$x = \chi \cos(\theta_s) + \xi_{sx}$$
$$y = \chi \sin(\theta_s) + \xi_{sy}.$$

A pixel $F_s(\chi, t)$ in the 2DST image is associated to pixel

$$I_s(\chi \cos(\theta_s) + \xi_{sx}, \chi \sin(\theta_s) + \xi_{sy}, t)$$

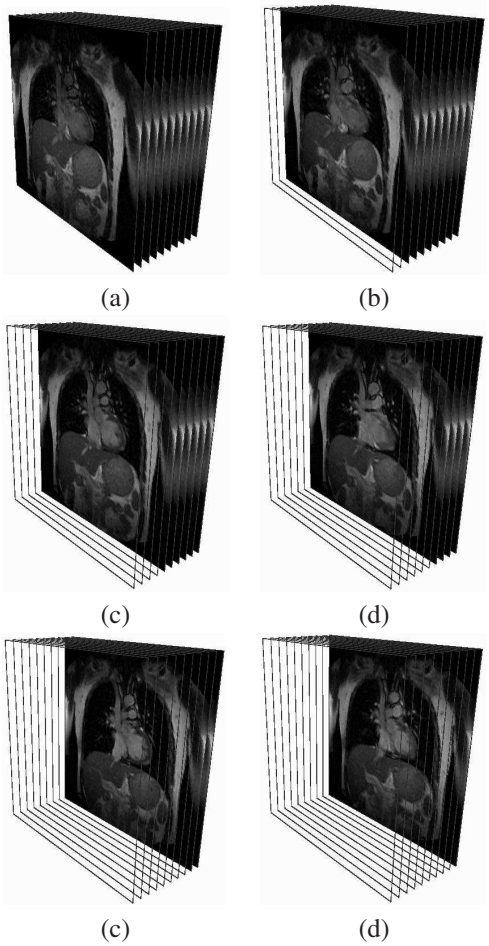

Figure 3. An example of one spatio-temporal volume (STV) builded from 10 MR images Im_{s,t_u}, $(u = 1, 2, 3..., 9)$ of a coronal slice s of the lung taken at time instants t_u. (a) STV with Im_{s,t_0} visible.(b) STV with Im_{s,t_2} visible.(c) STV with Im_{s,t_4} visible.(d) STV with Im_{s,t_6} visible.(e) STV with Im_{s,t_8} visible.(f) STV with Im_{s,t_9} visible.

in the original STV. The smallest value of time for $\min(f_s(t))$, named τ_s, defines the standard frame. Figure 4.(d) shows an ampliation of Figure 4.(a). The curve shown in Figure 4.(d) is dotted, showing the influence of the heart beating in the imaging.

3. Proposed Algorithm

The algorithm is divided in two steps: 2D respiratory motion analysis and 3D lung's reconstruction. In this work it is proposed a method that uses a sample function estimation to determine the presence of respiratory functions, it analyzes several values of θ_s in the range $[0^o, 360^o[$. One can check the result, and it is possible to correct the position of any point whenever necessary. The algorithm is re-applied if any correction where done. The second step is the creation of a B–Rep solid model of the lung, that is constructed in three steps: silhouette composition, mesh creation and corner creation. One can select one sequence of MR images, the B–Rep solid model of the lung associated to each image in the sequence is constructed, defining a 4D B–Rep solid model of the lung for the chosen STV.

3.1 Tracking the Respiratory Pattern

All images in the sequence are processed and the edges are determined using the Sobel operator that calculates the gradient of the image intensity at each point (mathematically, the gradient of a two–variable function is at each image point a 2D vector with the components given by the derivatives in the horizontal and vertical directions). Every image has its own set of edges. After the application of the Sobel operator the intensity of the edges is high.

The algorithm seeks the respiratory movement represented by $(\psi_{sx}(t), \psi_{sy}(t))$, associated with an arbitrary point ψ_s. However, as most organs move synchronously with breathing, the following expression can be written (Asakura et al., 2005):

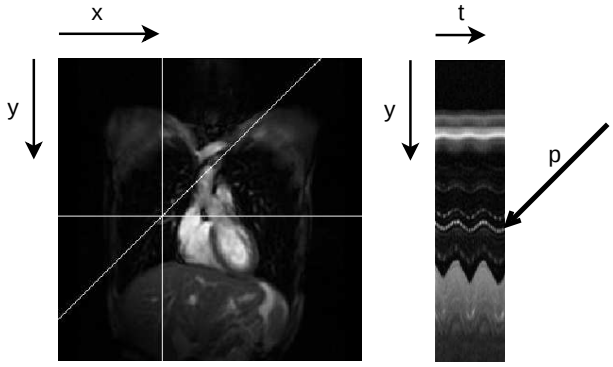

(a) Chest's MR Image and a vertical 2DSTI.

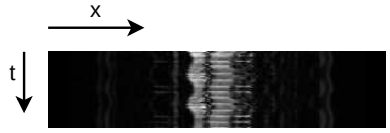

(b) A horizontal 2DSTI.

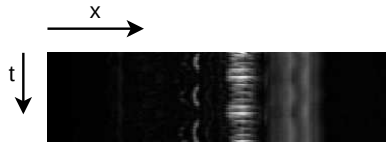

(c) An oblique 2DSTI.

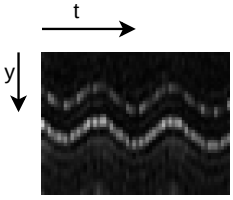

(d) Region showed by an arrow in (a).

Figure 4. A sample of a chest MR image and its 2D spatio temporal images (2DSTI). (a) shows a coronal image and a vertical 2DSTI. (b) shows a horizontal 2DSTI. (c) shows a diagonal 2DSTI. (d) shows a zoom from (a).

$$\begin{aligned}(\psi_{sx}(t), \psi_{sy}(t), t) &= (f_s(t)\zeta\cos\varphi + \psi_{sx}(\tau_s), \\ &\quad f_s(t)\zeta\sin\varphi + \psi_{sy}(\tau_s), t)\end{aligned} \tag{1}$$

where ζ and φ represents the scale and the orientation of the respiratory function associated to point ψ_s. The most suitable respiratory movement is searched, considering that the point belongs to the set of edges and the movement's coherence with $f_s(t)$. The search is done by varying ζ and φ (amplitude and angle). $(\psi_{sx}(t), \psi_{sy}(t), t)$ defines a sequence of pixels for a given ζ and φ. It is considered the pixel's intensity after the application of the Sobel operator. The average of the pixel's intensity must be high and the standard deviation must be low. Finally, the average and standard deviation are used in the following expression empirically determined:

$$E(\psi, \varphi, \zeta) = 0.9^{|\zeta|}\left(1 - \frac{S(\psi, \varphi, \zeta)}{3A(\psi, \varphi, \zeta)}\right) \tag{2}$$

where $A(\psi, \varphi, \zeta)$ and $S(\psi, \varphi, \zeta)$ represents the average and the standard deviation previously calculated. When the respiratory movement of $\psi_s(t)$ is in coherence with $f_s(t)$, the average of the edges's intensity is high and the standard deviation is low. Curves with shape similar to the diaphragm can have several candidates of respiratory movement with different angles and amplitudes. The algorithm seeks the candidate with smaller amplitude by penalizing greater values of ζ. The respiration movement associated to point $\psi_s(t)$ is given by $\max(E(\psi, \varphi, \zeta))$. Then it is possible to determine, for a given point, the angle and scale that best represent the respiratory function associated to it.

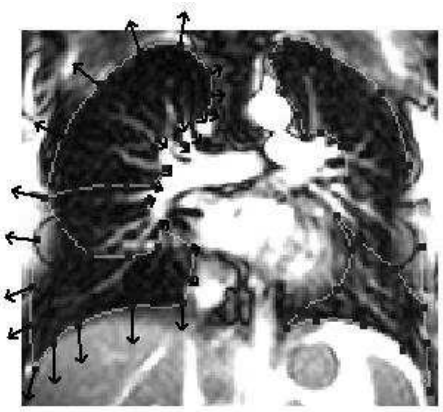

Figure 5. The scaled lung model.

3.2 Silhouette points as Scaled Functions

With the angle and scale that best represent the respiratory function $f_s(t)$ associated with each point $\mathbf{P}_{si}(\tau_s)$ that lies on the lungt's boundary in a given reference frame it is possible to estimate their position $\mathbf{P}_{si}(t)$ in other slices. The orientation and scale may be represented by a vector $\vec{\mathbf{v}}_{si}$ in the image space, according to the following expression:

$$\mathbf{P}_{si}(t) = \mathbf{P}_{si}(\tau_s) + \vec{\mathbf{v}}_{si} \cdot f_s(t) \tag{3}$$

where $\mathbf{P}_{si}(\tau_s)$ is a point in slice s from the standard frame, $\vec{\mathbf{v}}_{si}$ is a vector in the image space defined by the orientation and scale that best represent the respiratory function for this point, $f_s(t)$ is the respiratory function for slice s (see Figure 5).

For a given slice the respiratory function is working as a scale defining scaled lung's silhouettes in time. Then it is possible to simplify expression (3) by not considering the time, as

$$\mathbf{P}_{si}(\alpha) = \mathbf{P}_{si}(\tau_s) + \vec{\mathbf{v}}_{si} \cdot \alpha. \tag{4}$$

Using expression (4), one can determine a lung's silhouette in a slice s for a given scale α.

3.3 Reconstruction of the 3D Lung

The result from the 2D analysis is a set of silhouettes moving in time $\mathbf{S}_s(t)$. Although belonging to the same lung, each silhouette has its own time axis due to the long image acquisition time of MR systems, resulting in image sequences without coherence among them. The reconstruction of the 3D Lung is be accomplished through the interpolation between coronal and sagittal silhouettes considering the geometric information present in the DICOM images and the variation in the degree of breathing, in this work, the scale α given in expression (4).

3.3.1 Interpolation Criteria

In order to interpolate and match coronal and sagital silhouettes the following function is defined:

$$g_s(x, z, \alpha) = \|([M] \cdot \mathbf{S}_s(\alpha)) \bigcap line(x, z)\| \tag{5}$$

where $line(x, z)$ is a line parallel to the y axis and passing through coordinates x and z. Function $g_s(x, z, \alpha)$ returns the length of the edge defined by the intersection between the polygonal silhouette in the 3D space defined by $[M] \cdot \mathbf{S}_s(\alpha)$ and the straight line $line(x, z)$. $[M]$ is the matrix that converts the DICOM coordinates into the three dimensional space

$$\begin{bmatrix} p_x \\ p_y \\ p_z \\ 1.0 \end{bmatrix} = \begin{bmatrix} x_x \cdot \Delta_i & y_x \cdot \Delta_j & 0.0 & s_x \\ x_y \cdot \Delta_i & y_y \cdot \Delta_j & 0.0 & s_y \\ x_z \cdot \Delta_i & y_z \cdot \Delta_j & 0.0 & s_z \\ 0.0 & 0.0 & 0.0 & 1.0 \end{bmatrix} \cdot \begin{bmatrix} i \\ j \\ 0.0 \\ 1.0 \end{bmatrix} = [M] \cdot \begin{bmatrix} i \\ j \\ 0.0 \\ 1.0 \end{bmatrix} \tag{6}$$

where i and j are the column and row to the image plane. x_x, x_y and x_z are the row x direction cosine of the image orientation. y_x, y_y and y_z are the column y direction cosine of the image orientation. Δ_i is the column pixel resolution

Figure 6. Right and left lungs with its coronal silhouettes coherently composed.

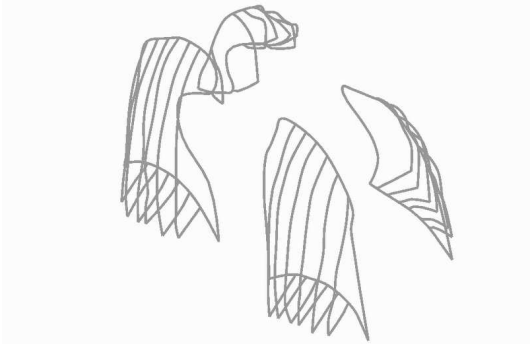

Figure 7. Right and left lungs with its sagittal silhouettes coherently composed.

and Δ_j is the row pixel resolution. s_x, s_y and s_z are the start position for the first voxel. Usually, coronal images have a bigger value for Δ_i and Δ_j when compared to sagittal images from the same patient.

3.3.2 Silhouette Composition

This section explains how to reconstruct the 3D lung associated to a given silhouette, using the acquired set of sagittal and coronal sequences of silhouettes. For simplification, it is assumed that a coronal silhouette is given; for a sagittal silhouette the method applies similarly. The coronal image contains the silhouettes for the right and left lung simultaneously. The sagittal images have a better quality when compared to the coronal images. However, the coronal images allow simultaneous reconstruction of the right and left lungs.

For a given coronal silhouette, a sagittal silhouette near the middle of the lung that fits the selected coronal silhouette according to the interpolation criteria is determined. This sagittal silhouette is used as guide, and coronal silhouettes that fits the determined sagittal silhouette are computed. This way, the right and left lungs are reconstructed simultaneously. This fit is given by the absolute position of the silhouette present in DICOM images (see equation 6) and the length of the silhouette intersection as function of the scale (see equation 5). Figure 6 shows an example of coronal silhouettes that fits to a determined sagittal silhouette. Next, sagittal silhouettes that fits the first and last coronal silhouettes are computed and clipped (Figure 7). The 3D lung skeleton is obtained (Figure 8).

Figure 8. Right and left lungs with their silhouettes coherently composed.

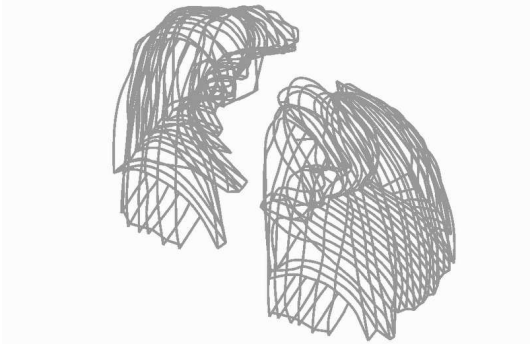

Figure 9. Right and left lungs with registered vertices connected by spans.

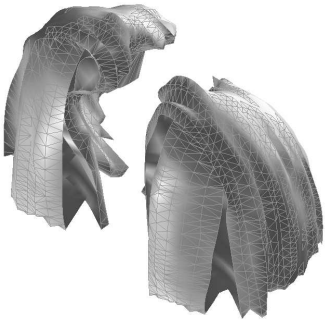

Figure 10. Right and left lungs with their mesh.

3.3.3 Mesh Creation

Now, it is necessary to create a B–Rep solid model of the lung, given a collection of planar silhouettes representing cross-sections. It is necessary to define the edges connecting the points from one silhouette to a point from a neighboring silhouette. This is known as tiling problem and is severely underconstrained (Meyers et al., 1992). Many surfaces could give rise to the observed cross-sections. In order to choose the "correct" surface, it is optimized with respect to some objective function. The chosen objective function should capture some notion of what a "good" surface is and should be easy to compute. Meyers et al. (1992) analyzed several objective functions. State of the art methods for shape reconstruction consider the possibilities of complex geometrical shapes and quick shape changes (Diebel et al., 2006; Liu et al., 2006; Paloc et al., 2006; Pauly et al., 2006), however this is not the case in this research.

When the cross sections are convex polygons a "good" surface can be easily created. However, the lung has concave polygons as cross sections. As a first step, neighboring silhouettes are registered by searching vertices with higher curvature and if two of them are near enough they are connected by the creation of edges named spans. Figure 9 shows the cross sections connected at registered vertices. Each edge in B-Rep solid model has two halfedges oriented in opposed directions (Mäntylä, 1988). Both halfedges from the spans connecting registered vertices are pushed into a stack and are used as initial halfedges in the meshing algorithm.

The B–Rep solid model is composed by vertices, edges and faces. Each vertex in the B-Rep solid model originated from a distinct silhouette. The intersection between sagittal and coronal silhouettes is an exception. It is associated an attribute to each vertex representing from which silhouette such vertex originated from. A span can only connect vertices from distinct silhouettes, i.e., vertices with different attributes.

Figure 10 shows the meshed right and left lungs. The algorithm created a surface interpolating sagittal and coronal neighboring silhouettes. Remains to define the four corners of the lung defined by sagittal and coronal silhouettes having only one neighboring silhouette.

Table 1. Characterizations of the three sequences of coronal and sagittal MR images used in the experiments

case	A	B	C
fov - cor (mm)	420×420	420×420	420×420
fov - sag (mm)	380×380	380×380	380×380
total time (s)	17	11	11
age	31	31	24

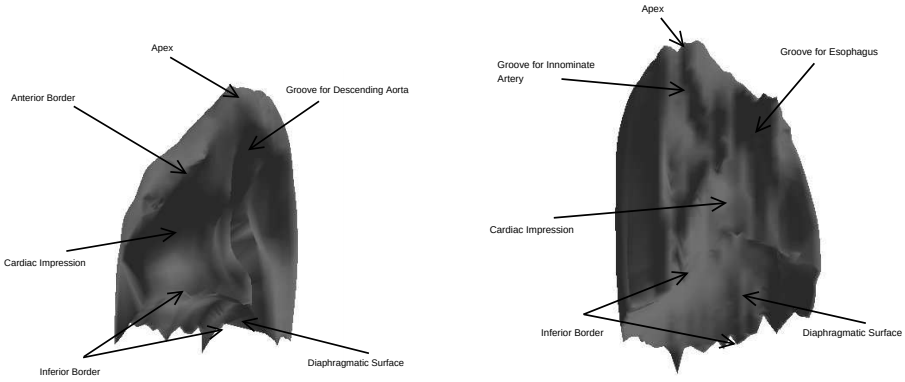

(a) Left lung characteristics. (b) Right lung characteristics.

Figure 11. (a) Mediastinal surface of the left lung and its characteristics. (b) Mediastinal surface of the right lung and its characteristics.

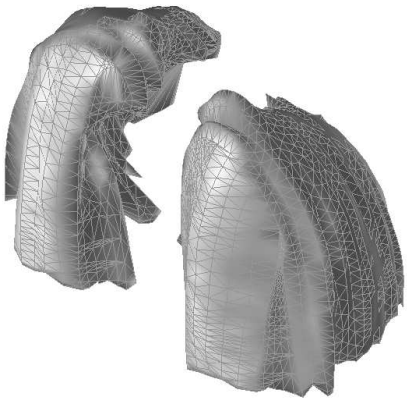

Figure 12. Lateral view of the right and left lungs shaded and meshed.

4. Results

The sequence of MR images used in the experiment were obtained by Symphony (1.5T) made by Siemens, using the method true FISP (Fast Imaging with Steady State Precession). The slice's thickness is 10 mm. It was used 22 coronal slices and 10 sagittal slices, with 256×256 pixels and 12 bits per pixel. The MR images were taken from three healthy non smoking persons. Table 1 shows some characterizations of the three sequences of MR images.

The three dimensional right and left lungs were created based on the selected sequence of MR images, the result can be seen in Figures 11.(a) and (b). It is possible to recognize several lung's characteristics in the three dimensional model. Figure 11.(a) shows the mediastinal surface of the left lung, and the following characteristics can be observed: apex, inferior border, cardiac impression, groove for descending aorta, anterior border and diaphragmatic surface. Figure 11.(b) shows the mediastinal surface of the right lung, and the following characteristics can be observed: apex, inferior border, cardiac impression, groove for esophagus and diaphragmatic surface. Figure 12 shows the shaded model of the left and right lungs with their mesh.

5. Acknowledgements

We would like to thank Prof. T. Inoue of Yokohama City University for useful suggestions. This research was partially supported by CNPq (second author) and JASSO (first author).

6. REFERENCES

Asakura, A., Gotoh, T., Kagei, S., Iwasawa, T. and Inoue, T., 2005, "Computer Aided System for Respiratory Motion Analysis of the Lung Region by Sequential MR Images.", *Medical Imaging Technology*, Vol. 23, Number 1, pp. 39–46, in Japanese.

Cluzel, P., Similowski, T., Chartrand-Lefebvre, C., Zelter, M., Derenne, J. P. and Grenier, P. A., 2000, "Diaphragm and

Chest Wall: Assessment of the Inspiratory Pump with MR Imaging-Preliminary Observations.", *Radiology*, Vol. 215, Number 2, pp. 574–583.

Diebel, J. R., Thrun, S. and Brünig, M., 2006, "A Bayesian Method for Probable Surface Reconstruction and Decimation.", *ACM Transactions on Graphics*, Vol. 25, Number 1, pp. 39–59.

DeCarlo, D., Kaye, J., Metaxas, D., Clarke, J. R., Webber, B. and Badler, N., 1995, "Integrating Anatomy and Physiology for Behavior Modeling.", *Medicine Meets Virtual Reality 3*, San Diego, 1995.

Gauthier, A. P., Verbatick, S., Estenn, M., Segebartg, C., Macklem, P. T. and Paiva, M., 1994, "Three Dimensional Reconstruction of the in Vivo Human Diaphragm Shape at Different Lung Volumes", *J Appl Physiol.*, Vol. 76, Number 2, pp. 495–506.

Gierada, D. S., Curtin, J. J., Erickson, S. J., Prost, R. W., Strandt, J. A. and Goodman, L. R., 1995, "Diaphragmatic Motion: Fast Gradient-Recalled-Echo MR Imaging in Healthy Subjects.", *Radiology*, Vol. 194, Number. 3, pp. 879–884.

Iwasawa, T., Kagei, S., Gotoh, T., Yoshiike, Y., Matsushita, K., Kurihara, H., Saito, K. and Matsubara, S., 2002, "Magnetic Resonance Analysis of Abonormal Diaphragmatic Motion in Patients with Emphysema.", *European Respiratory Journal*, Vol. 19, Number 2, pp. 225–331.

Ko, J. P. and Naidich, D. P., 2004, "Computer Aided Diagnosis and the Evaluation of Lung Disease.", *Thorac Imaging*, Vol. 19, Number 3, pp. 136–155.

Liu, Y. S., Paul, J. C., Yong, J. H., Yu, P. Q., Zhang, H., Sun, J. G. and Ramani, K., 2006, "Automatic Least–Squares Projection of Points onto Point Clouds with Applications in Reverse Engineering.", *Computer Aided Design*, Vol. 38, Number 12, pp. 1251–1263.

Mäntylä, M., 1988, *An Introduction to Solid Modeling*, Computer Science Press, Rockville, MD.

Meyers, D., Skinner, S. and Sloan, K., 1992, "Surfaces from Countours". *ACM Transactions on Graphics*, Vol. 11, Number 3, pp. 228–258.

Mills, G. H., Wild, J. M., Eberle, B. and van Beek, E. J. R., 2003, "Functional Magnetic Resonance Imaging of the Lung.", *British Journal of Anaesthesia*, Vol. 91, Number 1, pp. 16–30.

Paloc, C., Faraci, A. and Bello, F., 2006, "Online Remeshing for Soft Tissue Simulation in Surgical Training.", *IEEE Computer Graphics & Applications*, Vol. 26, Number 6, pp. 24–34.

Pauly, M., Kobbelt, L. P. and Gross, M., 2006, "Point–Based Multiscale Surface Representation.", *Transactions on Graphics*, Vol. 25, Number 2, pp. 177–193.

Promayon, E., Baconnier, P. and Puech, C., 1997, "Physically-Based Model for Simulating the Human Trunk Respiration Movements.", *In Lecture notes in Computer Science*, Springer Verlag, CVRMED II-MRCAS III first joint conference, Vol. 1205, pp. 379–388.

Ray, N., Acton, S. T., Altes, T., de Lange, E. E. and Brookeman, J. R., 2003, "Merging Parametric Active Contours Within Homogeneous Image Regions for MRI-Based Lung Segmentation.", *IEEE Transactions on Medical Imaging*, Vol.22, Number 2, pp.189–199.

Santhanam, A. P., Pattanaik, S. N., Fodopiastis, C. M., Hamza-Lup, F., Rolland, J. P. and Imielińska, C., 2004, "Physically-Based Deformation of High-Resolution 3D Models for Augmented Reality Based Medical Visualization.", *Augmented Environments for Medical Imaging-ARCS*, Rennes.

Suga, K., Tsukuda, T., Awaya, H., Takano, K., Koike, S., Matsunaga, N., Sugi, K. and Esato, K., 1999, "Impaired Respiratory Mechanics in Pulmonary Emphysema: Evaluation with Dynamic Breathing MRI.", *J Magn Reson Imaging*, Vol. 10, Number 4, pp. 510–520.

Tsui, B. M. W., Segars, W. P. and Lalush, D. S., 2000, "Effects of Upward Creep and Respiratory Motion in Myocardial SPECT.", *IEEE Transactions on Nuclear Science*, Vol. 47, pp. 1192-1195.

Zordan, V. B., Celly, B., Chiu, B. and DiLorenzo, P. C., 2004, "Breathe Easy: Model and Control of Simulated Respiration for Animation.", *Proceedings of the 2004 ACM SIGGRAPH/Eurographics symposium on Computer animation 2004*, Grenoble, France, 27–29.

7. Responsibility notice

The author(s) is (are) the only responsible for the printed material included in this paper